Protected Josephson Rhombus Chains

Matthew T. Bell,[1] Joshua Paramanandam,[1] Lev B. Ioffe,[1,2] and Michael E. Gershenson[1]
[1]Department of Physics and Astronomy, Rutgers University, Piscataway, New Jersey 08854, USA
[2]LPTHE, CNRS UMR 7589, 4 place Jussieu, 75252 Paris, France
(Received 26 November 2013; published 25 April 2014)

We have studied the low-energy excitations in a minimalistic protected Josephson circuit which contains two basic elements (rhombi) characterized by the π periodicity of the Josephson energy. Novel design of these elements, which reduces their sensitivity to the offset charge fluctuations, has been employed. We have observed that the lifetime T_1 of the first excited state of this quantum circuit in the protected regime is increased up to 70 μs, a factor of $\sim$100 longer than that in the unprotected state. The quality factor $\omega_{01}T_1$ of this qubit exceeds 10^6. Our results are in agreement with theoretical expectations; they demonstrate the feasibility of symmetry protection in the rhombus-based qubits fabricated with existing technology.

DOI: 10.1103/PhysRevLett.112.167001 PACS numbers: 74.50.+r, 03.67.Pp, 74.81.Fa, 85.25.Am

Quantum computing requires the development of quantum bits (qubits) with a long coherence time and the ability to manipulate them in a fault tolerant manner (see, e.g., Ref. [1] and references therein). Both goals can be achieved by the realization of a protected logical qubit formed by a collective state of an array of faulty qubits [2–7]. The building block (i.e., the faulty qubit) of the array is the Josephson element with an effective Josephson energy $E(\phi) = -E_2\cos(2\phi)$, which is π periodic in the phase difference ϕ across the element. In contrast to the conventional Josephson junctions with $E(\phi) = -E_1\cos(\phi)$, this element supports the coherent transport of pairs of Cooper pairs (the "4e" transport), whereas single Cooper pairs are localized and the "2e" transport is blocked [5,8,9]. Though this proposal has attracted considerable theoretical attention [10], the experimental realization of a protected qubit was lacking.

In this Letter we make an essential step towards building a protected Josephson qubit by fabricating the simplest protected circuit and demonstrating that the first excited state of the circuit is protected from energy relaxation.

The idea of protection is illustrated in Fig. 1. Let us consider the simplest chain of two $\cos(2\phi)$ elements. They share the central superconducting island whose charge is controlled by the gate. The Hamiltonian of this quantum circuit can be written as

$$H = -2E_2\cos(2\phi) + E_C(n - n_g)^2, \tag{1}$$

where the energy E_2 describes the Josephson coupling of the central superconducting island to the current leads, E_C is the effective charging energy of the island, n is the number of Cooper pairs on the island, n_g is the charge induced on the island by the gate. The parity of n is preserved if the transfer of single Cooper pairs is blocked ($E_1 = 0$, see Sec. I in the Supplemental Material [11]). In this case the states of the system can be characterized by the quantum number $\aleph = n \bmod (2)$. The low energy states corresponding to number $\aleph = 0, 1$ are shown in Fig. 1. The energy E_2 plays the role of the kinetic term that controls the "spread" of the wave functions along the n axis. Provided $E_2 \gg E_C$, the number of components with different n in these discrete Gaussian wave functions is large: $\langle n^2\rangle = \sqrt{E_2/E_C} \gg 1$, and the energy difference between the two states, $E_{01} = E_{|1\rangle} - E_{|0\rangle}$, is exponentially small (see Ref. [12] and Supplemental Material, Sec. I [11]):

$$E_{01} = 4A(g)g^{1/2}\exp(-g)\cos(\pi n_g)\omega_P. \tag{2}$$

Here $g = 4\sqrt{E_2/E_C}$, $\omega_P = 4\sqrt{E_2E_C}/\hbar$ is the plasma frequency, $A(g) \sim 1$ (Supplemental Material, Sec. I [11]). Furthermore, these states cannot be distinguished by the

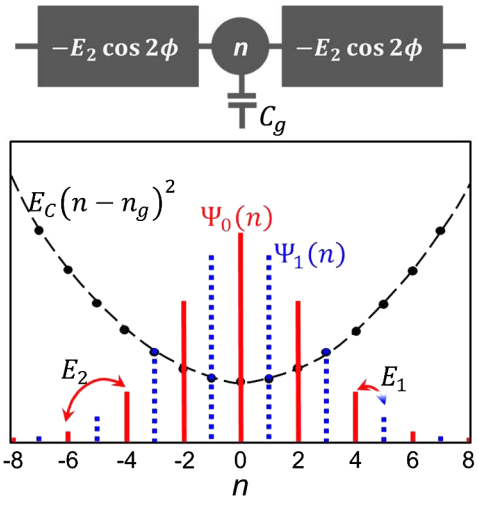

FIG. 1 (color online). Top panel: The chain of two $\cos(2\phi)$ elements; the charge of the central (common to both rhombi) island is controlled by the gate voltage. Bottom panel: Two lowest-energy wave functions in the discrete harmonic potential shown for $n_g = 0$.

noise operators, whose matrix elements acquire a small factor $\propto \exp(-g)$. Thus, the decay and dephasing rates are both reduced by the same factor $\propto \exp(-2g)$.

In real circuits, the $2e$ processes are not completely suppressed, and a nonzero amplitude E_1 mixes the odd and even components (Fig. 1) and increases E_{01}. For a small amplitude E_1 the decay of the first excited state is due to the mixture of $\aleph = 0$, 1 states and is suppressed by the factor $(2E_1/E_{01})^2 < 1$ in addition to the suppression by the factor $\exp(-2g)$ that is common to decay and dephasing. Thus, for the coherence protection two conditions are required: $E_2 \gg E_1$ (i.e., slow energy relaxation) and $E_2 \gg E_C$ (i.e., small dephasing rate).

The simplest $\cos(2\phi)$ Josephson element is represented by the Josephson rhombus: a superconducting loop interrupted by four identical Josephson junctions [5,8,9,13,14] [Fig. 2(a)]. When the rhombus is threaded by the magnetic flux $\Phi_R = \Phi_0/2$ (Φ_0 is the flux quantum), its effective Josephson energy $E_R = -E_{2R}\cos(2\phi)$ becomes π-periodic in the phase difference ϕ across the rhombus. In line with theoretical predictions, recent experiments [13] have demonstrated that the properly designed small rhombus arrays can support a nonzero $4e$ supercurrent in the regime when the $2e$ supercurrent vanishes.

In the current Letter, we have implemented the two-rhombus chain with an improved design of individual rhombi proposed in Ref. [12]. The key requirement for the protection is the cancellation of E_1 due to the destructive interference between the Cooper pair transfer amplitudes along the upper and lower branches of a rhombus.

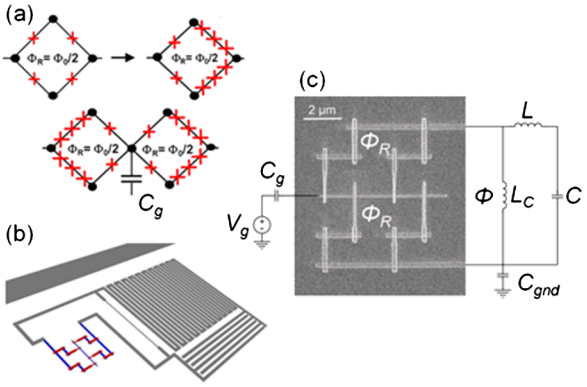

FIG. 2 (color online). Panel (a): The $\cos(2\phi)$ Josephson element (the Josephson rhombus) and its improved version which is less sensitive to the random offset charges on the upper and lower islands [12]. The chain contains two rhombi; the charge of the central (common to both rhombi) island is controlled by the gate voltage applied between the central conductor of the microstrip line and the ground. Panel (b): The on-chip circuit layout of the device inductively coupled to the microstrip transmission line. Panel (c): The micrograph of the two-rhombus chain coupled to the readout LC resonator via the kinetic inductance L_C of a narrow superconducting wire. The magnetic flux through each rhombus is Φ_R; the flux in the device loop is Φ.

This cancellation is difficult to achieve in the quantum regime where the amplitudes depend on the uncontrolled offset charges on the top and bottom islands. This dependence is due to the Aharonov-Casher effect (see, e.g., Ref. [15]) and the high probability of phase slips across the two small junctions in each arm of a rhombus. In the improved rhombus design [12] one junction in each branch is replaced by a short chain of larger junctions [Fig. 2(a)]. The phase slips across the larger junctions are suppressed due to a large $E_{\rm JL}/E_{\rm CL}$ ratio (50 for the studied devices). As a result, an improved rhombus becomes insensitive to the offset charges on all islands except for the central island shared by both rhombi. Below we refer to the characteristic energies of the smaller and larger junctions as $E_{\rm JS}$, $E_{\rm CS}$ and $E_{\rm JL}$, $E_{\rm CL}$ respectively. An optimal operation of the rhombus is realized for $E_{\rm JL} = mE_{\rm JS}$ and $E_{\rm CL} = E_{\rm CS}/m$, where m is the number of larger junctions in the chain ($m = 3$ for the studied devices).

The chains, the readout circuits, and the microwave (MW) transmission line were fabricated using multiangle electron-beam deposition of Al films through a lift-off mask (for fabrication details, see Refs. [16,17]). The in-plane dimensions of the small and large junctions were 0.14×0.13 μm^2 and 0.25×0.25 μm^2, respectively. The ratio $E_{\rm JS}/E_{\rm CS} \approx 3$–5 was chosen to realize the resonance frequency of the $|0\rangle \to |1\rangle$ transition, f_{01}, within the (1–10) GHz range. Below we show the data for one representative device with $E_{\rm JL} = 190$ GHz, $E_{\rm CL} = 4$ GHz, $E_{\rm JS} = 60$ GHz, and $E_{\rm CS} = 13$ GHz (throughout the Letter all energies are given in the frequency units, 20 GHz $\approx$ 1 K).

The readout lumped-element LC resonator was formed by the meandered 2-μm-wide Al wire with the inductance $L = 3$ nH and an interdigitated capacitor $C = 100$ fF. The resonator was coupled to the chain via a narrow superconducting wire with a kinetic inductance of $L_C = 0.4$ nH. The phase difference across the chain was controlled by the magnetic flux through the "device" loop formed by the chain and the coupling wire [Fig. 2(c)]. The global magnetic field, which determines the fluxes in both the device loop and the rhombus loops, has been generated by a superconducting solenoid; the field uniformity $\Delta B/B$ at the chip location was better than 10^{-4} cm^{-1}. Because the device loop area (1140 μm^2) was much greater than the rhombus area (13.5 μm^2), the phase across the chain could be varied at an approximately constant (within 2%) value of $\Phi_R = \Phi_0/2$. Several devices with systematically varied values of $E_{\rm JS}$ and $E_{\rm CS}$ were fabricated on the same chip and inductively coupled to the same microstrip line [Fig. 2(b)]. The devices could be individually addressed due to different resonance frequencies of the LC resonators. All measurements have been performed at $T = 20$ mK.

In the experiment, the microwaves traveled along the microstrip line inductively coupled to the device. The microwaves at the frequency ω_1 probed the LC resonance. The microwaves at the second-tone frequency ω_2 excited

the transitions between the quantum states of the chain, which resulted in a change of the impedance of this nonlinear system. The chain excitations were detected as a change in the amplitude $|S21|$ and the phase of the microwaves at the probe-tone frequency ω_1 (for measurement details, see Supplemental Material, Sec. II [11]).

Below we focus on the most interesting range of magnetic fields close to full frustration ($\Phi_R \approx \Phi_0/2$), where each rhombus represents a $\cos(2\phi)$ Josephson element. The measurements at the probe-tone frequency (no microwaves at ω_2) show that in this regime the response of the chain to the phase difference φ is indeed periodic with the period $\Delta\varphi = \pi$ (see Supplemental Material, Sec. III [11]).

Figure 3 summarizes the spectroscopic data obtained in the two-tone measurements. The inset shows the resonance frequency f_{01} measured as a function of n_g at a fixed magnetic flux $\Phi_R = 0.5\Phi_0$, $\varphi \approx 0$. Note that during the data acquisition time for the inset in Fig. 3 (~1.5 h), no long-term shifts in the offset charge were observed. The quasiparticle poisoning was strongly suppressed due to (a) a larger superconducting gap of the central island (in comparison with the nearest-neighbor islands) and a relatively large E_C [16,18], and (b) shielding of the device from stray infrared photons by the double-wall light-tight sample holder (see, e.g., Ref. [19]).

For perfectly symmetric rhombi, the two states corresponding to $\aleph = 0$, 1 (even and odd number of Cooper pairs on the central island) should become degenerate

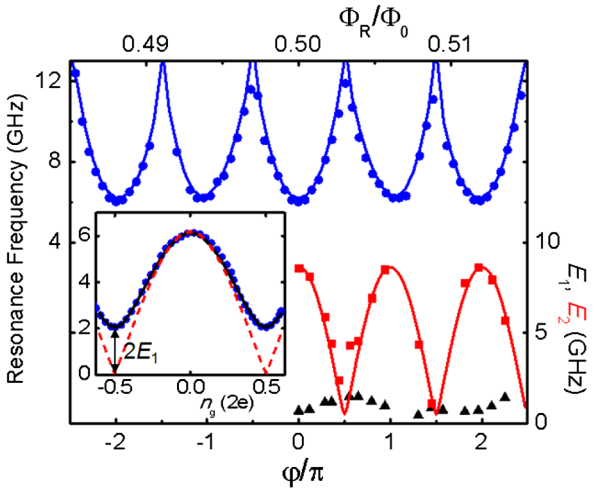

FIG. 3 (color online). The resonance frequency f_{01} (blue dots) and energies E_1 (black triangles) and E_2 (red squares) versus the phase φ across the chain near full frustration ($\Phi_R \approx 0.5\Phi_0$) at $n_g = 0$. The theoretical dependences $f_{01}(\varphi)$ (solid blue curve) and $E_2(\varphi)$ (solid red curve) were computed for $E_2 = 8.5$ GHz and $E_C = 15$ GHz. The inset: The dependence $f_{01}(n_g)$ at $\varphi = 0$ ($\Phi_R = 0.5\Phi_0$). The energies E_1 and E_2 were extracted from fitting the dependences $f_{01}(n_g)$ measured at different φ with the calculations based on Hamiltonian diagonalization (solid black curve). The expected dependence $f_{01}(n_g)$ for the case of perfectly symmetric rhombi is shown by the red dashed curve.

($f_{01} = 0$) at $n_g = \pm 0.5$. Slight asymmetry of the studied rhombus results in a nonzero $E_{01}(n_g = \pm 0.5) \approx 2E_1$ (see also Supplemental Material, Sec. IV [11]). At $n_g = 0$, $\varphi = \pi/2$ and $E_2 = 0$, E_{01} is equal to the effective charging energy $E_C = 15$ GHz. The nonzero energy E_2 suppresses E_{01} to 6 GHz (Fig. 3). The energies E_1, E_2, and E_C were obtained from the experimental dependences $f_{01}(n_g)$ measured at different values of φ by fitting them with the spectra obtained from numerical diagonalization of the Hamiltonian. The difference between the approximate analytical expression for E_{01} (2) and the result of numerical diagonalization is ~15%.

As a function of the phase difference across the chain, E_2 oscillates with the period $\Delta\varphi = \pi$ (Fig. 3). The dependence $E_2(\varphi)$ agrees very well with the one expected theoretically: $E_2(\varphi) = \sqrt{[2E_{2R}\cos(\varphi)]^2 + (\Delta E_{2R})^2}$ (solid red line) where $E_{2R} = 4.3$ GHz is the energy of an individual rhombus, ΔE_{2R} is the difference between the energies of the two rhombi. The fit shows that ΔE_{2R} does not exceed $0.1E_{2R}$ for the studied chain. The oscillations of E_2 result in a periodic dependence of the measured energy $E_{01}(\varphi)$. The estimated values of E_1 do not exceed 0.75 GHz around the values $\varphi = 0, \pi, \ldots$ corresponding to a maximum E_2. This small asymmetry in rhombus branches is consistent with the reproducibility of submicron junctions fabricated with the Manhattan-pattern technique [13,16,17].

Because the bandwidth of the second-tone microwave line in our setup was limited to 30 GHz, we could not access higher energy states directly. However, by increasing the second-tone power, we were able to observe the resonances corresponding to the multiphoton ($n = 2, 3, 4$) excitations of the $|0\rangle \rightarrow |2\rangle$ transition around the optimal values $\varphi = 0, \pi, \ldots$ The energy E_{02} extracted from these measurements exceeded 50 GHz which is in good agreement with our expectations, and confirms the validity of the theoretical model [Eq. (1)].

The energy relaxation of the state $|1\rangle$ was found by exciting the rhombus chain with a π pulse and then measuring its state after a variable time Δt [see Fig. 4(a) inset for pulse sequence]. The results of the energy relaxation measurements at the optimal working point ($\Phi_R = \Phi_0/2$, $\varphi = 0$) are presented in Fig. 4(a) and Table I. The optimal regime for the qubit corresponds to the maximum of E_2 (i.e., the maximum ($\sim g$) number of the odd/even components of the lowest-energy wave functions) and the strongest suppression of dephasing due to the

TABLE I. Characteristic parameters for protected (1) and unprotected (2) devices in the optimal regime ($\Phi_R = 0.5\Phi_0$, $\varphi = 0$).

Dev.	n_g	E_{01} (GHz)	$(2E_1/E_{01})^2$	$\mathcal{P}$	$\omega_{01}T_1$ (10^6)	T_1 (μs)
1	0	6	0.06	0.1	1.1	30
1	0.5	2	0.6	0.1	0.9	70
2	0.5	4	1	1	0.03	<1

charge noise [$\sim g^3 \exp(-2g)$]. The E_2 maxima are realized at $\varphi = 0, \pi, \ldots$, where E_2 becomes also insensitive (in the first order) to the flux noise in the device loop. At the same optimal values of φ we observed the minima of E_1, which also leads to the suppression of the fluctuations of E_2 and, thus, E_{01}. The decay rate due to the charge noise is expected to be suppressed by an additional factor $(2E_1/E_{01})^2$. For the studied (nonideal) device, this ratio does not depend strongly on φ: at both $\varphi = 0$ and $\varphi = \pi/2$ the ratio $(2E_1/E_{01})^2 \approx 0.06$ [$E_1(\varphi = \pi/2) \approx 1.5$ GHz, see Supplemental Material, Sec. IV [11]].

We also included in Table I the T_1 data for the device with a large degree of asymmetry (device 2). This asymmetry was caused by different values of the flux Φ_R in the nominally identical rhombi: variations of the magnetic field across the chip were caused by conventional (slightly magnetic) microwave connectors on the sample holder. After replacing these connectors with the nonmagnetic ones, this source of asymmetry was eliminated, and all the measured devices consistently demonstrated $T_1 \geq 30$ μs. The values of T_1 for the rhombus chains with a high degree of symmetry are 1–2 orders of magnitude greater than that for less symmetric rhombus circuits and unprotected Josephson qubits coupled to the same readout circuit [16,17].

The comparison shows that the symmetry protection suppresses the decay rate due to the charge noise by approximately 2 orders of magnitude, in agreement with the small value of the decay suppression factors, $(2E_1/E_{01})^2$ and $\mathcal{P} \approx g^3 \exp(-2g)$ (Table I). The latter estimate ignores the numerical preexponential factors $\sim O(1)$, for a more

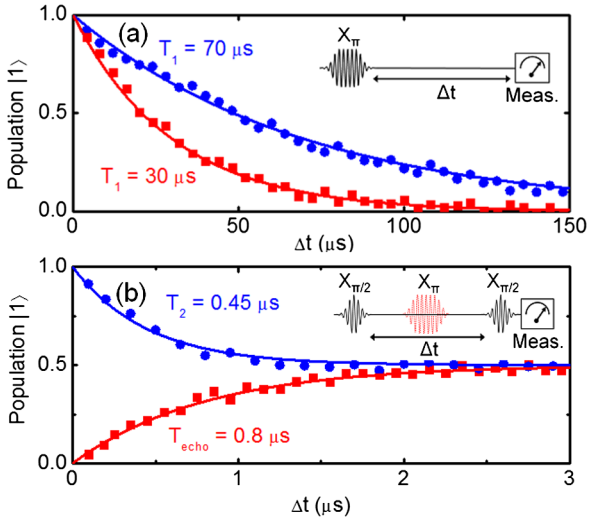

FIG. 4 (color online). The time-domain measurements at $\varphi = 0$ and $\Phi_R = 0.5\Phi_0$. Panel (a): Energy relaxation of the first excited state after application of a π pulse: $n_g = 0.5$ (blue circles), $n_g = 0$ (red squares). Inset: Pulse sequence used in the measurement. Panel (b): Ramsey (T_2) and spin echo (T_{echo}) measurements. Inset: Pulse sequence used in the measurements. For the spin echo measurement, a refocusing π pulse (red dashed line) was applied at $t = \Delta t/2$.

quantitative analysis see Supplemental Material [11], which includes Refs. [20–27]. The decay at $n_g = 0$ due to the charge noise is expected to be completely suppressed; the experimentally observed decay in this case is limited by the inductive coupling to the resonator and transmission line. For the detailed discussion of noises, see Supplemental Material, Sec. I [11], that also shows that at $\varphi = 0$ the dephasing is due to the flux noise in the individual rhombi.

The quality factor $\omega_{01}T_1$ for the protected rhombus chains exceeds 1×10^6 (see Table I), and is comparable with that for the state-of-the-art transmons coupled to 3D cavities [28] and resonators with interdigitated TiN capacitors [29]. However, the reasons for such a large $\omega_{01}T_1$ in the transmon and in the rhombus chain are different. The protection in our device is based on the smallness of the charge matrix elements between logical states, whereas in the transmon it is due to the smallness of the fluctuating electric potential associated with low density of states of the electromagnetic field.

In contrast to the long decay time, the decoherence time in the studied devices was relatively short (~ 1 μs). The time T_2 was determined in Ramsey measurements by applying an $X_{\pi/2}$ pulse followed by another $X_{\pi/2}$ pulse after a time Δt [see Fig. 4(b) inset for pulse sequence]. In the spin echo measurements, a refocusing X_π pulse was applied between the two $X_{\pi/2}$ pulses. From the Ramsey and spin echo measurements we found $T_2 = 0.45$ μs and $T_{\text{echo}} = 0.8$ μs. The dephasing time is expected to be long if $E_C \ll E_2$. In the studied chain, these energies were of the same order of magnitude, which resulted in significant dephasing [Fig. 4(b)].

To conclude, we have demonstrated that a Josephson circuit can be symmetry protected from the energy decay. We have studied the minimalistic protected circuit which contains two Josephson rhombi. The symmetry between the rhombus branches translates into halving of the periodicity of its Josephson energy $E(\phi) = -E_2 \cos(2\phi)$, and allows only the simultaneous transfer of pairs of Cooper pairs on the central island mutual to both rhombi. The logical states of the protected qubit correspond to the even and odd number of Cooper pairs on this island. Our data indicate that the improved design of the Josephson rhombi [12] reduces the sensitivity of the chain spectrum to the offset charge asymmetry. The measured phase and charge dependences of the energy of the $|0\rangle \rightarrow |1\rangle$ transition are in good agreement with our numerical simulations. Symmetry protection results in a long energy relaxation time T_1 (up to 70 μs) and a large quality factor $\omega_{01}T_1 > 10^6$ of this qubit. The experiments provide a solid foundation for the next stage—the implementation of a qubit with much improved coherence due to a larger ratio E_2/E_C.

We would like to thank B. Douçot for helpful discussions. The work was supported in part by grants from the Templeton Foundation (No. 40381), the NSF (No. DMR-1006265), and ARO (No. W911NF-13-1-0431).

[1] E. Knill, Nature (London) **434**, 39 (2005).
[2] A.Yu. Kitaev, Ann. Phys. (Amsterdam) **303**, 2 (2003).
[3] L. B. Ioffe, M. V. Feigelman, A. Ioselevich, D. Ivanov, M. Troyer, and G. Blatter, Nature (London) **415**, 503 (2002).
[4] L. B. Ioffe and M. V. Feigel'man, Phys. Rev. B **66**, 224503 (2002).
[5] B. Douçot and J. Vidal, Phys. Rev. Lett. **88**, 227005 (2002).
[6] B. Douçot, M. V. Feigelman, and L. B. Ioffe, Phys. Rev. Lett. **90**, 107003 (2003).
[7] B. Douçot, M. V. Feigelman, L. B. Ioffe, and A. S. Ioselevich, Phys. Rev. B **71**, 024505 (2005).
[8] I. V. Protopopov and M. V. Feigelman, Phys. Rev. B **70**, 184519 (2004).
[9] I. V. Protopopov and M. V. Feigelman, Phys. Rev. B **74**, 064516 (2006).
[10] P. Brooks, A. Kitaev, and J. Preskill, Phys. Rev. A **87**, 052306 (2013).
[11] See Supplemental Material at http://link.aps.org/supplemental/10.1103/PhysRevLett.112.167001, which includes Refs. [22–29], for technical aspects of the derivation of Eq. (2), analysis of coupling to different types of noises, and measurement procedures.
[12] B. Douçot and L. B. Ioffe, Rep. Prog. Phys. **75**, 072001 (2012).
[13] S. Gladchenko, D. Olaya, E. Dupont-Ferrier, B. Douçot, L. B. Ioffe, and M. E. Gershenson, Nat. Phys. **5**, 48 (2009).
[14] I. M. Pop, K. Hasselbach, O. Buisson, W. Guichard, B. Pannetier, and I. Protopopov, Phys. Rev. B **78**, 104504 (2008).
[15] I. M. Pop, B. Douçot, L. Ioffe, I. Protopopov, F. Lecocq, I. Matei, O. Buisson, and W. Guichard, Phys. Rev. B **85**, 094503 (2012).
[16] Matthew T. Bell, Lev B. Ioffe, and Michael E. Gershenson, Phys. Rev. B **86**, 144512 (2012).
[17] M. T. Bell, I. A. Sadovskyy, L. B. Ioffe, A. Yu. Kitaev, and M. E. Gershenson, Phys. Rev. Lett. **109**, 137003 (2012).
[18] J. Aumentado, Mark W. Keller, John M. Martinis, and M. H. Devoret, Phys. Rev. Lett. **92**, 066802 (2004).
[19] P. J. de Visser, J. J. A. Baselmans, P. Diener, S. J. C. Yates, A. Endo, and T. M. Klapwijk, Phys. Rev. Lett. **106**, 167004 (2011).
[20] J. Martinis, R. McDermott, M. Steffen, M. Ansmann, K. Osborn, K. Cicak, S. Oh, D. Pappas, R. Simmonds, and C. Yu, Phys. Rev. Lett. **95**, 210503 (2005).
[21] L. Faoro and L. B. Ioffe, Phys. Rev. Lett. **109**, 157005 (2012).
[22] D. Vion, A. Aassime, A. Cottet, P. Joyez, H. Pothier, C. Urbina, D. Esteve, and M. H. Devoret, Science **296**, 886 (2002).
[23] M. Metcalfe, E. Boaknin, V. Manucharyan, R. Vijay, I. Siddiqi, C. Rigetti, L. Frunzio, R. J. Schoelkopf, and M. H. Devoret, Phys. Rev. B **76**, 174516 (2007).
[24] N. A. Masluk, Ioan M. Pop, A. Kamal, Zl. K. Minev, and M. H. Devoret, Phys. Rev. Lett. **109**, 137002 (2012).
[25] A. Wallraff, D. I. Schuster, A. Blais, L. Frunzio, J. Majer, M. H. Devoret, S. M. Girvin, and R. J. Schoelkopf, Phys. Rev. Lett. **95**, 060501 (2005).
[26] S. Sendelbach, D. Hover, A. Kittel, M. Mück, J. M. Martinis, and R. McDermott, Phys. Rev. Lett. **100**, 227006 (2008).
[27] L. Faoro and L. Ioffe, Phys. Rev. Lett. **100**, 227005 (2008).
[28] Hanhee Paik, D. I. Schuster, L. S. Bishop, G. Kirchmair, G. Catelani, A. P. Sears, B. R. Johnson, M. J. Reagor, L. Frunzio, L. I. Glazman, S. M. Girvin, M. H. Devoret, and R. J. Schoelkopf, Phys. Rev. Lett. **107**, 240501 (2011).
[29] J. B. Chang, M. R. Vissers, A. D. Córcoles, M. Sandberg, J. Gao, D. W. Abraham, J. M. Chow, J. M. Gambetta, M. B. Rothwell, G. A. Keefe, M. Steffen, and D. P. Pappas, Appl. Phys. Lett. **103**, 012602 (2013).